Advances in Science and Technology Research Journal

*Advances in Science and Technology Research Journal*, 2027, 21(1), 180–192
https://doi.org/10.12913/22998624/231298
ISSN 2299-8624, License CC-BY 4.0

Received: 2026.07.21
Accepted: 2026.11.15
Published: 2026.12.01

# Study of the influence of electro-spark deposition process parameters and a comparative analysis of microscopy and computed tomography in the qualitative assessment of copper coatings on an aluminium substrate

Piotr Młynarczyk[1*], Damian Bańkowski[1], Wojciech Depczyński[1]

[1] Department of Materials Science and Materials Technology, Faculty of Mechatronics and Mechanical Engineering, Kielce University of Technology, al. 1000-lecia P.P. 7, 25-314 Kielce, Poland
* Corresponding author's e-mail: piotrm@tu.kielce.pl

## ABSTRACT

This article presents research into surface coatings produced by the electro-spark deposition (ESD) method on aluminium using a copper electrode. ESD is a surface modification technique that uses short current pulses (electrical discharges) to transfer material from the working electrode (anode) to the workpiece (cathode). The evaluation involved observing the effect of voltage and capacitor capacitance during the ESD process on the thickness of the ESD coating. To minimise the number of experiments required, a two-factor, five-level Hartley experimental design was selected. The study demonstrates the potential use of computed tomography to monitor the condition of the resulting ESD coating. Unlike previous studies, where the evaluation of ESD coatings was mainly based on the analysis of single metallographic cross-sections, in this work computed tomography was used for three-dimensional, non-destructive evaluation of the coating continuity and geometry, as well as quantitative analysis of its thickness. VG Studio software enables visualisation of the resulting ESD coating, including measurement of its thickness or volume. Microscopic observations were then carried out on the prepared samples to analyse the thickness and structure of the coatings. The use of tomographic studies in the analysis of ESD coatings ensures significantly greater representativeness of the results compared to traditional microscopy. It allows for a spatial assessment of the coating's continuity, which eliminates the risk of misinterpreting quality based on individual cross-sections. Furthermore, the spatial data obtained form the basis for precise mathematical models, enabling a better understanding of the process's energy balance and more accurate prediction of ESD coating thickness as a function of process parameters. The scientific novelty of this work is the three-dimensional analysis of the obtained coatings using the ESD method, as opposed to the previously performed analyses of metallographic cross-sections.

**Keywords:** electro-spark deposition, computed tomography, microscopic examination, coatings.

## INTRODUCTION

In recent years, there has been a rapidly growing interest in the industry in innovative coating application technologies and the regeneration of critical components. The key requirements for these processes are high safety, reliability, economic efficiency and low environmental impact [1–3]. Conventional deposition methods such as HVOF, PVD, CVD and electroplating, commonly used to improve the wear and corrosion resistance of parts, are, however, fraught with significant drawbacks. These include high equipment costs, considerable time consumption and the generation of pollutants [4–6]. Furthermore, these techniques prove unsuitable for thermally sensitive structural materials (e.g. aluminium and magnesium alloys), which are widely used in the aerospace industry. This is due to the fact that high heat input causes the formation of an extensive heat-affected zone (HAZ), residual stresses and deformation [1, 5–10]. These phenomena

directly lead to the degradation of the mechanical properties of the finished components. A coating produced by the electro-spark deposition (ESD) method is strongly metallurgically bonded to the substrate, and the process itself is characterised by low thermal input, a narrow HAZ and low remanufacturing costs. Thanks to these advantages, this technology has become a widely used method of surface engineering. Furthermore, due to the high costs of sintered parts or tools, economical alternatives for their regeneration are being sought. Among the many available solutions, the ESD technique stands out for its low operating costs and versatility, enabling the repair of tools using a variety of coating materials [11–14]. It allows for the local strengthening or regeneration of components in order to restore – and even exceed – the original quality and performance parameters of the parts. This solution enables the effective extension of the service life of parts and tools. Electroslag surfacing is a pulsed microwelding process in which short-duration electrical discharges with high current density are used to deposit fusible electrode material onto a metal substrate. The ESD technique utilises a pulsed spark discharge between the metal substrate and the electrode, enabling the electrode material to melt and infiltrate the surface layer of the metal substrate, forming a deposited surface alloy coating with special properties and a metallurgical bond to the substrate [15–17]. This treatment optimises the physicochemical properties of the substrate surface and, to some extent, improves the hardness, wear resistance and corrosion resistance of the original substrate material [18].

This process can be carried out automatically or by manual application of the coating by an operator. The surface after coating application is not smooth and uniform; this is due to the melting and deposition of material from the electrode. Often, if the parameters are not selected appropriately, cracks [19] or porosity may be observed in the resulting surface coating.

The scientific literature extensively describes the influence of process parameters on surface roughness [20,21], the thickness of the produced coatings [22], as well as on improving their hardness, resistance to abrasive wear [23–25] or corrosion resistance [25,26]. Coating thickness is most commonly assessed on the basis of microscopic examination or by the gravimetric method, by determining the increase in the sample's mass. However, these approaches do not provide a complete geometric characterisation of the coating. Microscopic analysis is limited to randomly selected cross-sections measured at several points, whilst gravimetric measurements may be subject to significant error. This is because the mass balance does not account for the loss of substrate material due to its ablation (evaporation) under the influence of discharges, making it impossible to accurately determine the actual amount of material transferred from the electrode.

The aim of this article is a comparative assessment of the thickness of coatings deposited by the ESD method, carried out using classical optical microscopy and X-ray computed tomography (micro-CT). The analysis was supplemented by gravimetric studies, including measurements of mass changes in both the samples and the working electrodes before and after the treatment process. The scientific contribution of this study is the integration of micro-CT-based three-dimensional coating characterization with Hartley experimental design and response surface methodology (RSM), enabling a quantitative evaluation of the relationship between ESD process parameters and coating thickness compared to OM testing.

## MATERIALS

The material used in the study was aluminium A1 (AW-1050A), onto which a Cu-ETP copper coating was applied. Aluminium samples with a diameter of 25 mm and a height of 10 mm were prepared for the tests. The samples were then subjected to ESD treatment using a copper electrode; the process is illustrated in Figure 1.

The layers were deposited using various parameters described in the experimental plan (Table 2). As the aim is to measure the thickness of the deposited coating, its surface area and deposition time must be strictly controlled, whilst minimising the operator's influence on the experiment. Upon completion of the experiment, the deposition thickness is measured directly, without any surface treatment.

### Tomographic examination

Micro-CT (micro-computed tomography) examinations were carried out using the NIKON M2 LES measurement system (Figure 2). The

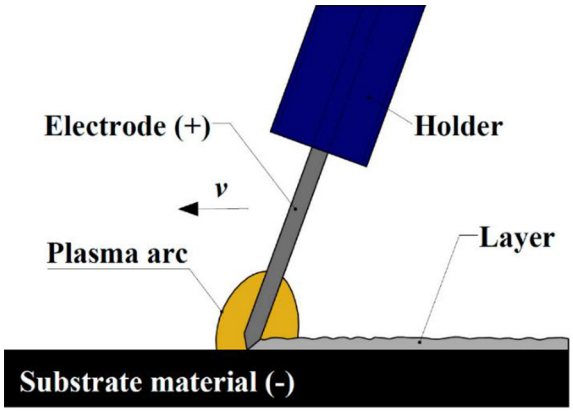



**Figure 1.** Schematic diagram of surface coating formation by electrospark deposition [27]

system was equipped with an X-ray tube featuring a rotating tungsten anode, operating at a maximum accelerating voltage of 225 kV. Radiographic data were recorded using a VAREX XRD 1611 XP flat-panel digital detector with a 4048 × 4048 pixel matrix and a pixel size of 0.1 mm. Three-dimensional (3D) reconstruction based on two-dimensional (2D) shadow projections was performed using the dedicated Inspect-X software, version V6.8. Structural analysis of cross-sections and quantitative measurements of the tungsten coating thickness were carried out using Volume Graphics software [28].

The essence of the research method employed is based on recording the intensity of X-rays passing through the structure of the object under investigation. The detection of subtle differences in the radiographic density of individual areas of the material allows for precise mapping of the component under investigation [29]. Consequently, this technique enables the identification of applied material coatings. The decrease in the intensity of radiation reaching the detector surface is a function of the material's density and the path travelled by the beam[30]. The exposure parameters are presented in Table 1.

After scanning, all samples were processed in the Inspect-X programme, and then, using Volume Graphics software, the surface of the coating obtained by ESD treatment was created and thickness measurements were taken. An example of a coating measurement is shown in Figure 3.

## Metallographic examination

In order to assess the microstructure of the deposited coating, the samples examined by computed tomography were cut transversely to produce metallographic sections. The samples were embedded in Technovit 5000 conductive epoxy resin, taking care to ensure they were not skewed. The surface preparation process was carried out in two stages. Preliminary grinding was carried

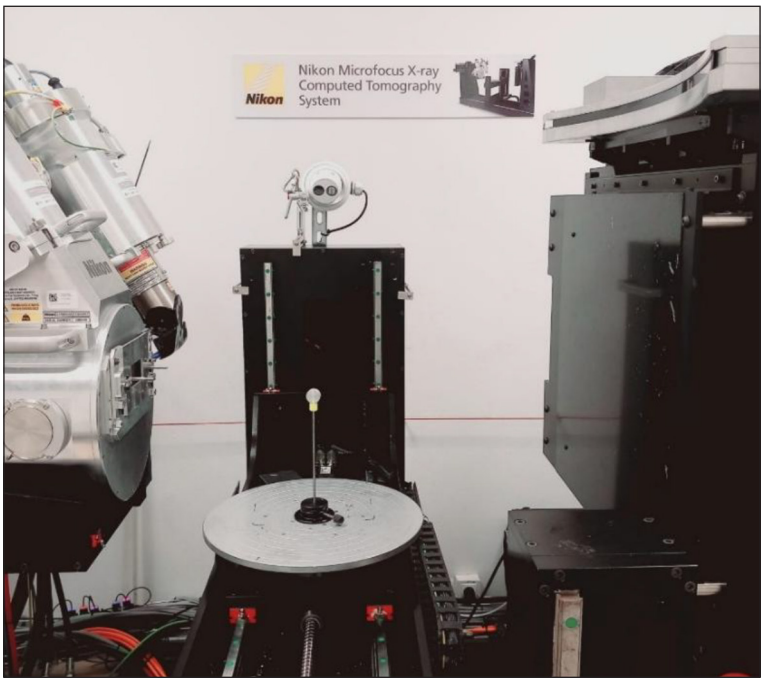



**Figure 2.** NIKON M2 LES computed tomography system

**Table 1.** X-ray exposure parameters

| Parameter | Value |
|---|---|
| Voltage | 190 kV |
| Current | 295 µA |
| Power | 56.1 W |
| Filter | No |
| Voxel size | 18.0 µm |
| Projection | 1520 |
| Time per projection | 708 ms |

out on a Presi Minitech 263 grinder-polisher using silicon carbide (SiC) abrasive papers with the following grit sizes: 230, 400, 600, 1200 and 2500. Final polishing was carried out on a Struers LaboPol-5 machine using SUPRA polishing cloth and a polycrystalline diamond suspension with a particle size of 1 µm.

Microstructural analysis of the cross-sections was carried out using a Nikon Eclipse MA 200 inverted metallographic microscope, in conjunction with NIS-Elements Viewer image analysis software (version AR 6.1). The thickness of the deposited coating was determined using a statistical method: for each sample, a minimum of three measurements were taken at five randomly selected locations, and the mean value was then calculated. An example microphotograph from the measurements is shown in Figure 4.

### Hartley's two-factor, five-level planned experiment

Due to the need to limit the number of experimental trials, a two-factor, five-level Hartley experimental design was selected, which was dictated by the desire to investigate the influence of independent variables on the output parameters over a wider range than is the case with three-factor designs. Statistica 10 software (64-bit version) was used to generate the design and perform statistical analysis of the results. The ranges of variation in process parameters for the individual coded levels:

- voltage, U, took the values 300, 400, 500, 600, 700, which correspond respectively to the code values: -1.414; -1; 0; 1; 1.414
- capacitor capacitance – f took the values 25, 33, 50, 75, 133, which correspond to the code values: -1.414; -1; 0; 1; 1.414

## RESULTS

Based on the experimental data obtained, response surfaces were developed in Statistica for the functions of changes in the thickness of the coatings obtained, as well as changes in electrode mass and sample mass as a function of voltage and capacitor capacitance. It was possible to

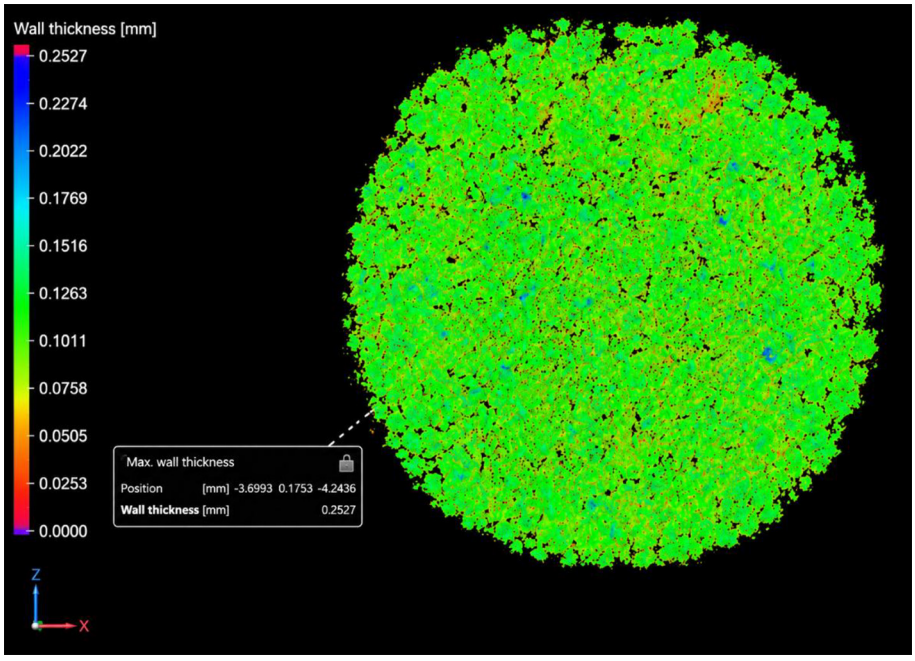



**Figure 3.** View of the 3D CT model of the resulting coating, together with a thickness analysis and the maximum thickness of the coating marked. Parameters: voltage 600 V, 50 µF

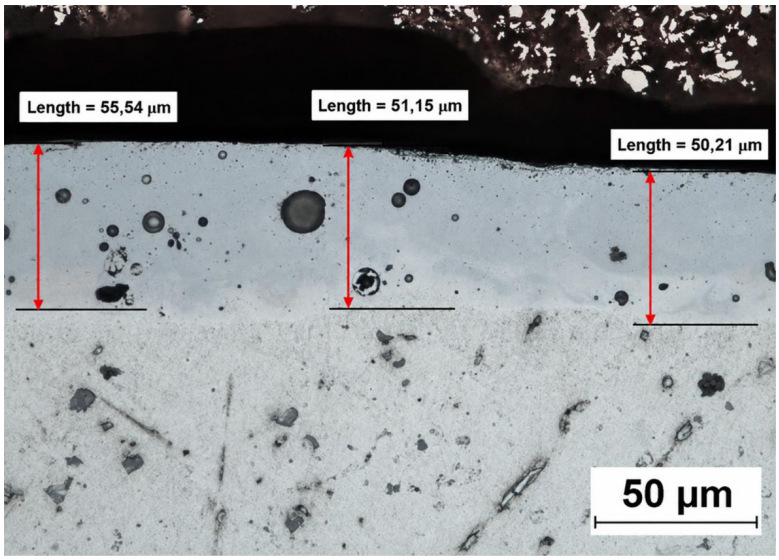



**Figure 4.** Microphotograph showing the thickness of the deposited layer, 500×, parameters: voltage 400 V, 25 µF

**Table 2.** Hartley's five-level two-factor experimental design

| No. | Capacitor capacitance, [µF] | Voltage, [V] | CT layer thickness, [µm] | SD of CT measure-ments | Microscopic observation layer thickness, [µm] | SD of OM measure-ments | ΔmE, [mg] | ΔmW, [mg] |
|---|---|---|---|---|---|---|---|---|
| 1 | 25 | 400 | 53.8 | 2.4 | 48.2 | 2.6 | 33.2 | 14.3 |
| 2 | 50 | 400 | 71.5 | 2.6 | 64.5 | 2.9 | 72.6 | 39.2 |
| 3 | 25 | 600 | 78.6 | 2.7 | 68.4 | 3.2 | 30.7 | 8.6 |
| 4 | 50 | 600 | 110.7 | 4.2 | 105.2 | 4.4 | 66.8 | 17.7 |
| 5 | 75 | 300 | 103.3 | 3.9 | 95.6 | 4.1 | 47 | 19.5 |
| 6 | 75 | 700 | 121.9 | 5.6 | 120.2 | 5 | 77.9 | -10.4 |
| 7 | 50 | 500 | 94.4 | 3.8 | 101.1 | 4.1 | 45.5 | 6 |
| 8 | 133 | 500 | 131 | 6.8 | 128.5 | 5.7 | 98.7 | 1.8 |
| 9 | 75 | 500 | 125.8 | 5.8 | 118.6 | 6 | 81.8 | 24.1 |
| 10 | 75 | 500 | 125 | 5.6 | 120.1 | 6.1 | 81.4 | 23.8 |

determine the mathematical relationships between the input parameters and the measured output values by applying response surface methodology (RSM) within the adopted experimental design.

Furthermore, mathematical models of changes in coating thickness and changes in the masses of the sample and electrode were generated for each graph using Statistica software. In addition, an analysis of variance (ANOVA) was performed, taking into account the effects of individual terms of the quadratic equation and the interaction of input factors on the model. Due to the nature of the experiment, no ANOVA analysis was performed with backward analysis analysis of the influence of individual factors for the adopted significance level α. For the resulting equations, correlation coefficients R were determined, reflecting the variability of the studied feature in the resulting approximation equation. This allows for a clear assessment of the effectiveness of regression fitting models. The correlation coefficient is a numerical measure of the degree to which two or more variables are interdependent. Furthermore, the coefficient of determination $R^2$ and the adjusted coefficient of determination $R^2$-adj were determined for each equation. The $R^2$ coefficient values are a statistical measure of how close the predicted data are to the fitted regression line. As part of the analysis of the obtained results, the percentage of influence of individual terms of the regression equations on the model was also determined. This work will form part of the team's future research into coatings produced by ESD methods. The team envisages

conducting an experiment combining all possible levels without limiting the number of replicates required to carry out the experiments. This work aims to demonstrate the influence of individual ESD process factors on coating formation and the differences between measurements using an optical microscope and computed tomography.

The significance of regression equation terms and the recommendation to reject terms that have no impact on the model are determined using Student's t-testing for a given significance level of α. This level is typically set at α = 0.05 [27,31]. Verification involves rejecting terms for which the p-value exceeds the assumed significance level, and considering terms with a p-value below α in the equation. Analyzing Tables 3–6 reveals that in most models, the linear and quadratic dependencies of F (capacitor capacitance) achieved p-values below 0.05, simultaneously having the greatest impact on the model. Interactions between factors were very low due to the physics of the process. High energies (as the product of voltage and capacitor capacitance) delivered to the samples cause uncontrolled melting and evaporation of the material without affecting the thickness of the layers formed.

In order to graphically illustrate the relationship between the input factors and the individual quality indicators – coating thickness and mass loss of the electrode and the sample – in the ESD coating process, surface fits were used in the Statistica software. These enabled the creation of graphs showing the relationship between individual process indicators and capacitor capacitance and voltage – Figures 5–8.

The ESD coating formation mechanism is governed by the energy delivered during individual spark discharges. Although the spark energy can be estimated from the electrical parameters of the discharge circuit, the subsequent phenomena, including heat transfer, melting, evaporation, plasma formation, and material transport, are highly transient and mutually dependent. Therefore, these phenomena are considered as consequences of the discharge energy rather than independent process parameters. Increasing the discharge energy may increase the amount of molten electrode material transferred to the substrate;

**Table 3.** Results of the ANOVA analysis for the thickness of the deposited copper coating measured under a microscope

| Parameter | Sum of squares (SS) | Number of degrees of freedom | Mean square | F | P | influence % |
|---|---|---|---|---|---|---|
| Model | 4659.94 | 5 | 4659.94 | - | - | |
| F | 3301.282 | 1 | 3301.282 | 41.68166 | 0.002964 | 70.84% |
| $F^2$ | 896.506 | 1 | 896.506 | 11.31920 | 0.028190 | 19.24% |
| U | 160.375 | 1 | 160.375 | 2.02488 | 0.227825 | 3.44% |
| $U^2$ | 93.314 | 1 | 93.314 | 1.17818 | 0.338767 | 2.00% |
| FU | 208.463 | 1 | 208.463 | 2.63203 | 0.180047 | 4.47% |
| Error | 316.809 | 4 | 79.202 | | | |
| Total SK | 6267.040 | 9 | $R^2$=0.95 | | $R^2$ - adj = 0.89 | |

**Table 4.** Results of the ANOVA analysis of the thickness loss of the manufactured copper coating measured by computed tomography

| Parameter | Sum of squares (SS) | Degrees of freedom | Mean square | F | P | influence % |
|---|---|---|---|---|---|---|
| Model | 1761.223 | 5 | 1761.223 | - | - | |
| F | 1424.389 | 1 | 1424.389 | 65.32821 | 0.001273 | 80.87% |
| $F^2$ | 131.832 | 1 | 131.832 | 6.04636 | 0.069771 | 7.49% |
| U | 135.984 | 1 | 135.984 | 6.23675 | 0.066956 | 7.72% |
| $U^2$ | 63.875 | 1 | 63.875 | 2.92958 | 0.162136 | 3.63% |
| FU | 5.143 | 1 | 5.143 | 0.23587 | 0.652607 | 0.29% |
| Error | 87.214 | 4 | 21.804 | | | |
| Total SK | 2044.189 | 9 | $R^2$=0.96 | | $R^2$ - adj = 0.90 | |

however, the final coating thickness also depends on heat dissipation, plasma dynamics, and the efficiency of material deposition.

The graph shows that for low voltages of around 250 V, the thickness of the copper coating produced increases significantly as the

**Table 5.** Results of the ANOVA analysis of the mass changes of the electrode

| Parameter | Sum of squares (SS) | Number of degrees of freedom | Mean square | F | P | influence % |
|---|---|---|---|---|---|---|
| Model | 4087.075 | 5 | 4087.075 | - | - | |
| F | 2762.197 | 1 | 2762.197 | 17.96843 | 0.013275 | 67.58% |
| $F^2$ | 376.285 | 1 | 376.285 | 2.44778 | 0.192740 | 9.21% |
| U | 439.539 | 1 | 439.539 | 2.85926 | 0.166111 | 10.75% |
| $U^2$ | 307.625 | 1 | 307.625 | 2.00114 | 0.230090 | 7.53% |
| FU | 201.429 | 1 | 201.429 | 1.31032 | 0.316176 | 4.93% |
| Error | 614.900 | 4 | 153.725 | | | |
| Total SK | 4785.544 | 9 | $R^2$=0.87 | | $R^2$ - adj = 0.71 | |

**Table 6.** Results of the ANOVA analysis for changes in sample weight

| Parameter | Sum of squares (SS) | Number of degrees of freedom | Mean square | F | P | influence % |
|---|---|---|---|---|---|---|
| Model | 1229.298 | 5 | 1229.298 | - | - | |
| F | 159.877 | 1 | 159.8768 | 1.200733 | 0.334722 | 13.01% |
| $F^2$ | 279.754 | 1 | 279.7536 | 2.101050 | 0.220793 | 22.76% |
| U | 467.520 | 1 | 467.5198 | 3.511242 | 0.134235 | 38.03% |
| $U^2$ | 306.096 | 1 | 306.0964 | 2.298894 | 0.204055 | 24.90% |
| FU | 16.051 | 1 | 16.0514 | 0.120552 | 0.745935 | 1.31% |
| Error | 532.598 | 4 | 133.1494 | | | |
| Total SK | 1712.364 | 9 | $R^2$=0.69 | | $R^2$ - adj = 0.30 | |

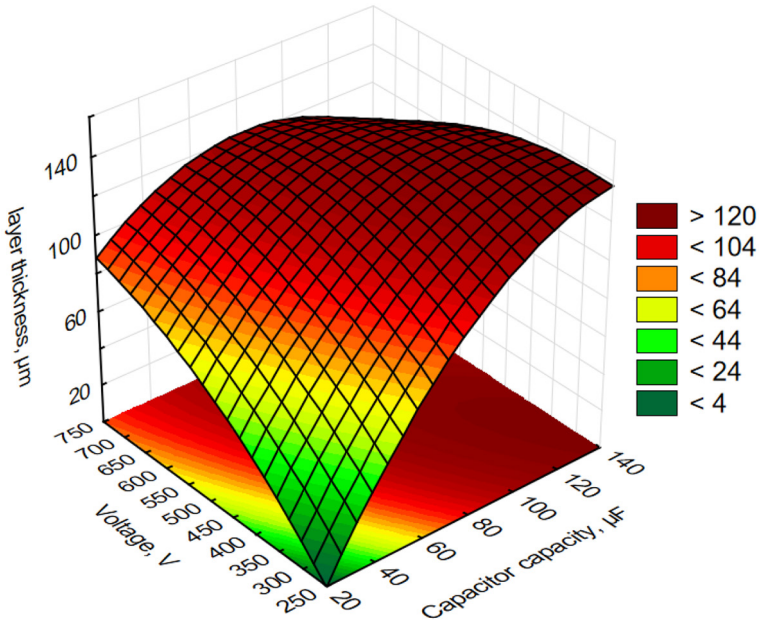



**Figure 5.** Estimated changes in coating thickness obtained from computed tomography as a function of voltage and capacitor capacitance during the production of copper coatings. The observed trend confirms that the capacitor capacitance has a greater influence than the voltage

capacitor capacitance increases. For voltages ranging from 250 V to 500–600 V, the thickness of the copper coating also increases; however, once the capacitance exceeds 100–120 μF, the increase in thickness remains constant. For high voltages in the range of 600–750 V, the graph takes on a completely different character: as the capacitor's capacitance increases up to 100 μF, the thickness of the recorded coatings increases, but once 100 μF is exceeded, the coating thickness decreases. It can also be inferred from the graph that the use of higher voltages at low capacitor capacitance results in an increase in the thickness of the analysed copper coatings. The situation is completely different for high capacitor capacitance (140 μF); in this case, as the ESD process voltage increases, the coating thickness decreases.

Based on the measurements carried out and the graph of coating thickness obtained from microscopic observations as a function of capacitor capacitance and voltage during the ESD copper coating process, it can be seen that the nature of the graph is analogous to the data obtained from tomographic measurements. Despite the similar nature of the graphs, it can be observed that the tomographic measurements showed coating thicknesses approximately 5.14% greater than the coating thicknesses obtained from microscopic observations. Due to the negligible difference in density, computed tomography (CT) examinations do not allow for the distinction between the deposited layer and the portion of the diffusion layer rich in intermetallic compounds and phases. It is very possible that this situation causes CT scans to reveal a thicker layer of deposit than microscopic examinations.

Based on the graph, it can be concluded that both an increase in voltage and an increase in capacitor capacitance result in an increase in the mass loss of the working electrode. This has a physical basis, as an increase in voltage results in higher energy and faster evaporation of the working electrode.

The graph shows the process parameters at which an increase or decrease in sample mass occurs. The greatest increases in sample mass are observed at approximately 350 to 450 V and capacitances ranging from 40 to 80 uF. An undesirable decrease in sample mass occurs when voltages above 600 V are applied. High voltages and large capacitor capacitances result in the dissolution of the sample due to high-energy discharges. Although the observed thickness of the deposited coating increases, this occurs at the expense of the dissolution and evaporation of the substrate material. It should be noted that both the electrode and the sample, made of

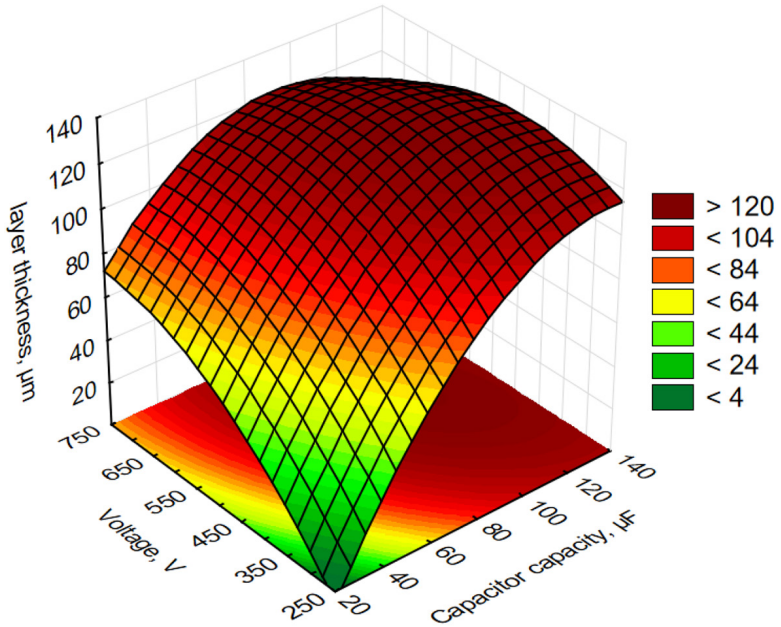



**Figure 6.** Estimated changes in coating thickness obtained from microscopic observations as a function of voltage and capacitor capacitance during the production of copper coatings
This graph indicates that capacitor capacitance is a more important factor in determining film thickness than voltage

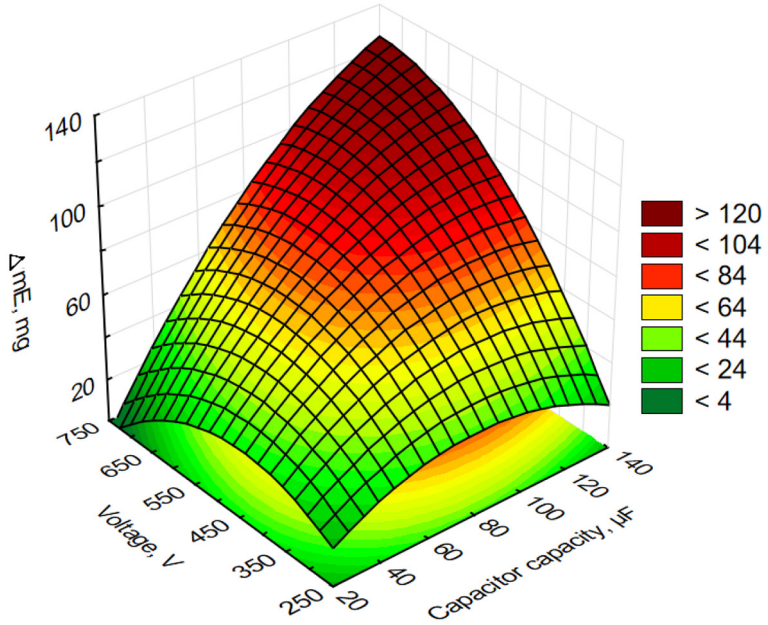



**Figure 7.** Estimated electrode mass loss as a function of voltage and capacitor capacitance during the production of copper coatings
The graph shows that both capacitor capacitance and voltage have a similar effect on electrode wear in the analyzed range of parameters

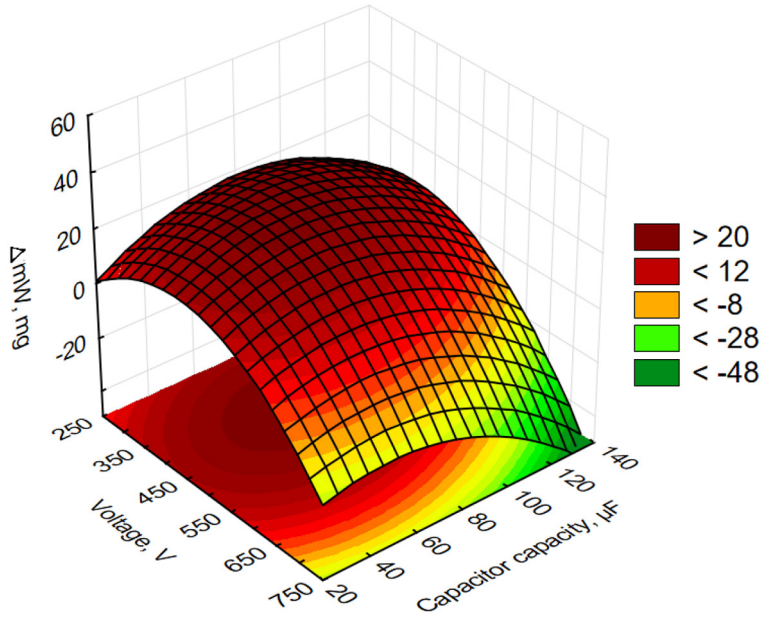



**Figure 8.** Estimated changes in sample mass as a function of voltage and capacitor capacitance during the production of copper coatings
The observed trend indicates that voltage has a greater effect on the mass change of the object than the capacitor capacitance. Furthermore, the use of high voltages and capacitances reduces the mass of the sample by introducing very high energy, intensely melting,and evaporating the material

copper and aluminium respectively, are characterised by excellent conductivity and thermal capacity. However, the sample material has a significantly lower melting and boiling point than the electrode material.

The derived forms of the equations for coating thickness and mass changes of the sample and electrode for the ESD process of copper on an aluminium substrate, as well as the correlation coefficients, coefficients of determination

and adjusted coefficients of determination, are presented in Table 7.

The equations obtained for the thickness of the formed coatings and the mass changes of the electrode are characterised by a very high correlation coefficient R of over 0.9, whilst for the mass increase of the sample, the correlation coefficient R takes the value of 0.83.

The calculated percentage contributions of individual input factors of the ESD treatment process to the models indicate that the thickness of the formed copper coatings is most strongly influenced by the linear relationship of the capacitor capacitance. The remaining terms and their mutual interactions are less significant, typically accounting for a few to a dozen or so per cent.

The accuracy of the developed models was verified through residual analysis. Examination of the plots of the expected value versus the experimental value – Figures 9 – reveals a linear relationship. This indicates a good model of the dependence on voltage and capacitor capacitance for ESD treatment.

The relationship between residuals and predicted values shown in Figures 10 demonstrates the random nature of the residuals. The analyses carried out confirm the adequacy of the regression models developed.

**Table 7.** Regression equations developed for the parameters of the copper coating process

| Form of the regression equation | R | $R^2$ |
|---|---|---|
| $t_{CT} = -143.31 + 3.03 \cdot C - 0.008 \cdot C^2 + 0.44 \cdot U - 0.0002 \cdot U^2 - 0.002 \cdot C \cdot U$ | 0.97 | 0.95 |
| $t_M = -151.02 + 2.81 \cdot C - 0.009 \cdot C^2 + 0.47 \cdot U - 0.0002 \cdot U^2 - 0.001 \cdot C \cdot U$ | 0.98 | 0.96 |
| $\Delta m_E = -50.74 + 0.35 \cdot C - 0.005 \cdot C^2 + 0.31 \cdot U - 0.0004 \cdot U^2 + 0.002 \cdot C \cdot U$ | 0.93 | 0.87 |
| $\Delta m_W = -78.80 + 0.91 \cdot C - 0.005 \cdot C^2 + 0.37 \cdot U - 0.0004 \cdot U^2 - 0.0006 \cdot C \cdot U$ | 0.83 | 0.69 |

**Note:** U – Voltage, V; C – Capacitor capacitance, µF; $t_{CT}$ – coating thickness from tomographic examination, µm; $t_M$ – coating thickness from microscopic examination, µm.

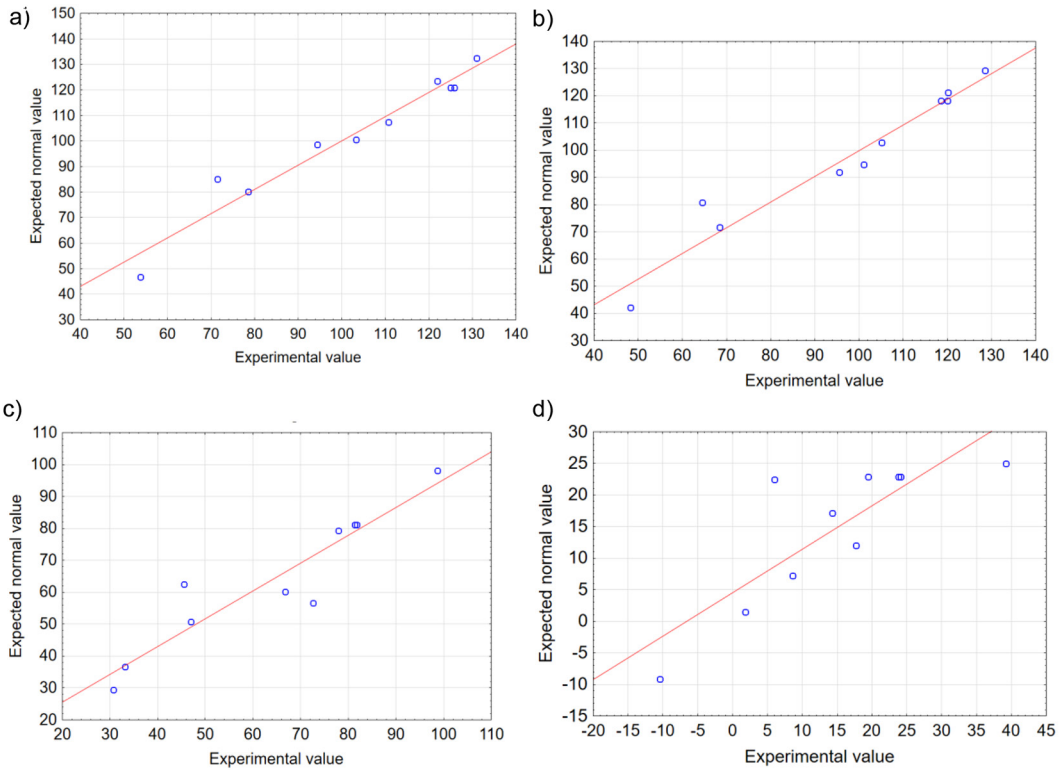



**Figure 9.** Analysis of residuals of the approximated values relative to the observed values for the model of a) coating thickness obtained from tomographic studies, b) coating thickness obtained from microscopy, c) electrode mass loss, d) change in sample mass. Linear relationships confirm the good fit of the models to the observed real data

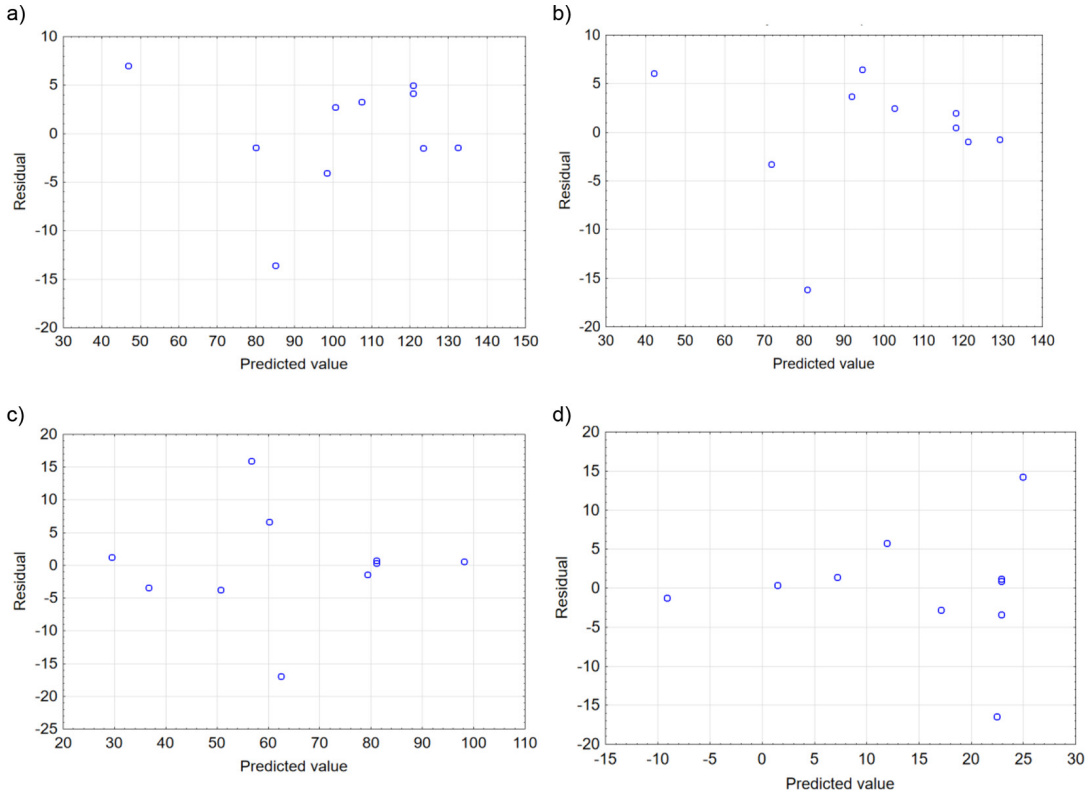



**Figure 10.** Analysis of residuals relative to the estimated values for the model: a) coating thickness obtained from tomographic studies, b) coating thicknesses obtained from microscopy, c) electrode mass loss, d) change in sample mass. Randomly placed points indicate the random nature of the residuals

## CONCLUSIONS

The results obtained indicate that coatings measured using a computed tomography scanner are on average 5% thicker than those measured by optical microscopy. This is because computed tomography averages all the results. The average thickness for measurement 4 from the CT scan was 110.7 µm, whilst the maximum thickness of this coating at a single point reached 0.2527 µm – more than twice as much. This was probably due to greater transfer of the electrode fragment. The average from the CT measurements would have been greater than 5% had it not been for measurement 7, in which a thicker coating was observed in the microscopic examinations than in the tomographic examinations.

It can be unequivocally stated that computed tomography is suitable for rapid and non-destructive coating measurement; however, the deposited material must have a different density from the substrate material to facilitate identification. Microscopic examinations provide better information regarding the quality of the coating obtained and allow for analysis of the phases present.

For the effective production of copper coatings, low capacitor capacitances in the range of 40 to 80 µF should be used; the choice of voltage in the range of 300 to 500 V may be dictated by other technological considerations (e.g. surface roughness), as it does not significantly affect the mass efficiency of the process. However, given the thickness of the deposited coatings, capacitances in the range of 80–100 µF and a voltage of 450 to 600 V should be used. Parameters of 80 µF and 500 V can be the most favorable conditions within the analyzed test range, as indicated by the response surface analysis.

The mass results for the electrode and the workpiece clearly show that at high process parameters, the greatest evaporation of the substrate material and the working electrode occurs, and negative mass gains were recorded.

It should be emphasised that the ESD process was performed manually, which introduces uncontrolled variability in electrode movement, which may affect coating thickness and microstructure. At the same time, manual deposition offers certain advantages, particularly in exploratory and laboratory research. It provides greater

flexibility and adaptability, allowing the operator to adjust the electrode position and contact pressure in real time.

## REFERENCES


1. Paydas, H.; Mertens, A.; Carrus, R.; Lecomte-Beckers, J.; Tchuindjang, T. Laser cladding as a repair technology for Ti–6Al–4V alloy: Influence of building strategy on microstructure and hardness. Mater. Des. 2015, 85, 497–510.
2. Renna, G.; Leo, P.; Casavola, C. Effect of electrospark process parameters on the WE43 magnesium alloy deposition quality. Appl. Sci. 2019, 9, 4383. https://doi.org/10.3390/app9204383
3. Felix, L.M.; Kwan, C.C.; Zhou, N.Y. The effect of pulse energy on the defects and microstructure of electro-spark-deposited Inconel 718. Metall. Mater. Trans. A 2019, 50, 4223–4231.
4. Cao, T.; Lei, S.; Zhang, M. The friction and wear behaviour of Cu/Cu-$MoS_2$ self-lubricating coating prepared by electrospark deposition. Surf. Coat. Technol. 2015, 270, 24–32.
5. Feldshteina, E.E.; Kardapolova, M.K.; Gaida, R.; Khorodyski, B.; Kaval'chuk, O.V. Tribological properties of electrospark-deposited and further laser-hardened coatings. J. Frict. Wear 2013, 34, 137–141.
6. Renna, G.; Leo, P.; Cerri, E.; Zanon, G.P. Thermal shock behaviour of CoCrAlTaY coatings on a Ni-base superalloy. Metall. Ital. 2015, 107, 33–41.
7. Brandt, M. Laser Additive Manufacturing: Materials, Design, Technologies, and Applications; Woodhead Publishing: Cambridge, UK, 2016.
8. Barile, C.; Casavola, C.; Pappalettera, G.; Pappalettere, C. Analysis of crack propagation in stainless steel by comparing acoustic emissions and infrared thermography data. Eng. Fail. Anal. 2015, 69, 35–42.
9. Mao, Y.; Li, Z.; Feng, K.; Guo, X.; Zhou, Z.; Wu, Y. Corrosion behaviour of carbon film-coated magnesium alloy with an electroless plating nickel interlayer. J. Mater. Process. Technol. 2015, 219, 42–47.
10. Ermakova, E.N.; Sysoev, S.V.; Nikulina, L.D.; Tsyrendorzhieva, I.P.; Rakhlin, V.I.; Kosinova, M.L. Synthesis and characterisation of organosilicon compounds as novel precursors for CVD processes. Thermochim. Acta 2015, 622, 2–8.
11. Liu, Y.; Qu, J.; Cai, X.; Zhang, W.; Zhang, S. Experimental study on electro-spark additive/subtractive repair for worn cemented carbide. Machines 2023, 11, 333. https://doi.org/10.3390/machines11030333
12. Senin, P.V.; Velichko, S.A.; Martynov, A.V.; Martynova, E.G. Increasing the wear resistance of forged tools by electrospark deposition. Russ. Eng. Res. 2020, 40, 427–430.
13. Sychev, A.P.; Kolesnikov, I.V.; Sycheva, M.A. Extending the life of frictional components in freight cars by hybrid electrospark deposition. Russ. Eng. Res. 2022, 42, 49–52.
14. Tarelnyk, V.B.; Gaponova, O.P.; Myslyvchenko, O.M.; Sarzhanov, B.O. Electrospark deposition of multilayer coatings. Powder Metall. Met. Ceram. 2020, 59, 76–88.
15. Wang, J.; Zhang, M.; Dai, S.; Zhu, L. Research progress in electrospark deposition coatings on titanium alloy surfaces: A short review. Coatings 2023, 13, 1473. https://doi.org/10.3390/coatings13081473
16. Koshuro, V.; Fomina, M.; Fomine, A.; Rodionov, I. Metal oxide (Ti, Ta)–(TiO2, TaO) coatings produced on titanium using electro spark alloying and modified by induction heat treatment. Compos. Struct. 2018, 196, 1–7.
17. Wang, D.; Gao, J.; Deng, S.; Wang, W. A novel particle planting process based on electrospark deposition. Mater. Lett. 2022, 306, 130872.
18. Manakova, O.S.; Kudryashov, A.E.; Levashov, E.A. On the application of dispersion–hardened SHS electrode materials based on (Ti, Zr)C carbide using electrospark deposition. Surf. Eng. Appl. Electrochem. 2015, 51, 413–421.
19. Bańkowski D., Młynarczyk P. Visual testing of casting defects after vibratory machining. Archives of Foundry Engineering. 2020; 4/2020, 72–7. https:// doi.org/10.24425/afe.2020.133350
20. Haponova, O.; Tarelnyk, V.; Mościcki, T.; Tarelnyk, N. Hybrid surface treatment technologies based on the electrospark alloying method: a review. Coatings 2025, 15, 721. https://doi.org/10.3390/coatings15060721
21. Mlynarczyk, P.; Spadlo, S. The analysis of the effects of the formation of an iron–tungsten carbide layer on an aluminium alloy by the electrical discharge alloying process. In Proceedings of the 25th Anniversary International Conference on Metallurgy and Materials (METAL), Brno, Czech Republic, 25–27 May 2016; pp. 1109–1114.
22. Li, B.; Ma, X.; Liu, Y.; Wang, H.; Bao, M.; Wang, R. Research on the Ultrasonic Electro-Spark Deposition Process and the Properties of the Deposition Layer. Coatings 2025, 15, 1038. https://doi.org/10.3390/coatings15091038
23. Madej, M.; Radon-Kobus, K.; Milewski, K.; Drabik, S.; Piotrowska, K.; Kowalczyk, J. Tribological properties of diamond-like-carbon coating doped with tungsten. Metalurgija 2024, 63, 85–88.

24. Radek, N.; Bartkowiak, K. Laser treatment of Cu–Mo electro–spark deposited coatings. Phys. Procedia 2011, 12, 499–505.
25. Kostadinov, G.; Nikolov, A.; Sofronov, Y.; Penyashki, T.; Mishev, V.; Tzaneva, B.; Dimitrova, R.; Petrov, K.; Miltchev, R.; Gavrilov, T. Tribological and corrosion properties of coatings of ultradisperse TiB2-TiAl electrodes with nanosized additives deposited on Ti-Gr2 by non-contact electrospark deposition. Materials 2026, 19, 1652. https://doi.org/10.3390/ma19081652
26. Scendo, M.; Spadlo, S.; Staszewska-Samson, K.; Mlynarczyk, P. Influence of heat treatment on the corrosion resistance of aluminium-copper coating. Metals 2020, 10, 966.
27. Młynarczyk, P.; Bańkowski, D.; Depczyński, W. The Impact of Selected ESD Parameters on the Properties of Tungsten Layers. Materials 2025, 18, 4581. https://doi.org/10.3390/ma18194581
28. Bańkowski, D.; Nowakowski, Ł.; Skrzyniarz, M.; Błasiak, S.; Kurp, P.; Depczyński, W.P.; Młynarczyk, P.S. Evaluating the impact of the tool and additional fruit cutting on changes in pitted cherries using digital volume correlation with computed tomography. Adv. Sci. Technol. Res. J. 2025, 19, 162–175.
29. Bay, B.K. Methods and applications of digital volume correlation. J. Strain Anal. Eng. Des. 2008, 43, 745–760.
30. Depczyński, W.P.; Bańkowski, D.; Młynarczyk, P.S. Computed tomography and scanning electron microscopy analysis of a friction stir welded Al-Cu joint. Arch. Foundry Eng. 2023, 23, 65–71.
31. Bańkowski, D.; Młynarczyk, P.; Depczyński, W. Comparative studies of the effectiveness of rotational and vibratory machining. Materials 2026, *19*, 1554. https://doi.org/10.3390/ma19081554